Electrochimica Acta 112 (2013) 252–257

Contents lists available at ScienceDirect

Electrochimica Acta

journal homepage: www.elsevier.com/locate/electacta

Combination of acid-resistor and -scavenger improves the SEI stability and cycling ability of tin–nickel battery anodes in $LiPF_6$-containing electrolyte

Myeong-Ho Choo[a,1], Cao Cuong Nguyen[b,1], Sukhyun Hong[a], Yo Han Kwon[c], Sang-Wook Woo[c], Je Young Kim[c], Seung-Wan Song[a,b,*]

[a] Graduate School of Green Energy Technology, Chungnam National University, Daejeon 305-764, Republic of Korea
[b] Department of Fine Chemical Engineering & Applied Chemistry, Chungnam National University, Daejeon 305-764, Republic of Korea
[c] Battery R & D, LG Chem, Ltd., Daejeon 305-380, Republic of Korea

ARTICLE INFO

Article history:
Received 20 May 2013
Received in revised form 5 August 2013
Accepted 19 August 2013
Available online 11 September 2013

Keywords:
Rechargeable lithium batteries
Anode
Tin
Interfacial control
Solid electrolyte interphase

ABSTRACT

Control of electrode–electrolyte interfacial reactivity and the formation of the solid electrolyte interphase (SEI) layer is a key technology for high performance rechargeable lithium batteries. Here we present the first report on a promising interfacial approach for Sn–Ni electrode that the use of acid-resisting and -scavenging fluorine-dopant on Sn combined with acid-scavenging trimethyl phosphite electrolyte additive to $LiPF_6$-contiaing carbonate-based organic electrolyte improves the interfacial stability of Sn to acidic electrolyte species. As a result, a stable SEI layer consisting of a plenty of carbonate decomposition products forms and cycling ability significantly improves, in contrast to less efficient SEI formation and rapid performance fade for the electrodes without fluorine-dopant or trimethyl phosphite additive.

1. Introduction

Tin (Sn)-based materials have received a particular attention as alternative anode materials to graphite because of about three times higher theoretical capacity (997 mAh g^{-1}) than that of graphite [1] and appropriate operating voltage above lithium. Distinct advantages of Sn are a high electronic conductivity and a handy fabrication using soft chemical routes to enable the construction of tin anode-embedded batteries in diverse architectures, as demonstrated in our recent report regarding a cable-type flexible lithium-ion battery [2]. Sn, however, suffers from a rapid performance fade due to significant volume change by up to 300% upon repeated lithiation (charge) and delithiation (discharge) cycles [1]. A variety of methods for improving cycling ability of Sn-based anodes have been reported, mostly in a manner which utilizes homogeneous mixing with various carbon (*e.g.* graphite), nanostructured Sn-carbon composites [3–7], carbon-coating [8] or core–shell structure [9].

As another cause responsible for a poor performance is an interfacial instability of Sn in conventional electrolyte [10,11], where $LiPF_6$ produces various acids in the presence of a trace of water; $LiPF_6 \leftrightarrows PF_5 + LiF$, $PF_5 + H_2O \rightarrow 2HF + PF_3O$ [12,13]. The loss of active Sn upon etching by HF and the deactivation of Sn by electrophilic attack of strong Lewis acids PF_5 and PF_3O should be detrimental in sustaining its structure and cycling performance [10–12]. Irreversible formation of acid-derived surface species continues with cycling while experiencing a dynamic variation in active interfacial area by cracking or agglomeration of Li_xSn particles [14]. The formation of a stable solid electrolyte interphase (SEI) layer seems to be hardly obtainable on Sn in conventional electrolyte. Relatively little report on interfacial (SEI) control of Sn-based anode is available. The combinative use of fluoroethylene carbonate and vinylene carbonate as electrolyte additives on micro-TiSnSb anode by Wilhelm et al. [15], which was formulated with carboxymethyl cellulose binder and carbon fiber, showed improved cycle life but the effect of additives on the SEI of the anode was not explained.

The demanding strategy to overcome the interfacial problem is the inhibition of both HF-etching and attack of Lewis acids. For the studies of interfacial control and surface chemistry, we use carbon- and polymer binder-free film model electrodes, which

---

* Corresponding author at: Department of Fine Chemical Engineering & Applied Chemistry, and Graduate School of Green Energy Technology, Chungnam National University, Daejeon 305-764, Republic of Korea. Tel.: +82 42 821 7008; fax: +82 42 822 6637.
E-mail address: swsong@cnu.ac.kr (S.-W. Song).

[1] These authors contributed equally.

0013-4686/$ – see front matter © 2013 Elsevier Ltd. All rights reserved.
http://dx.doi.org/10.1016/j.electacta.2013.08.121

provide high-quality IR and X-ray photoelectron spectroscopic (XPS) data and a precise characterization of the SEI composition [10,11,16–18]. Clearer insights into electrode–electrolyte interfacial processes than in bulk electrodes can be attained.

Here, we report for the first time a promising interfacial approach to improve the cycling ability of tin–nickel (Sn–Ni) electrode through a small fraction of fluorine (F)-doping on Sn and the use of trimethyl phosphite ($P(OCH_3)_3$) electrolyte additive. The effects of interfacial control on the SEI stability and cycling ability of Sn–Ni electrode are discussed.

2. Experimental

The 450–550 nm thick films of F-free and F-doped Sn–Ni were deposited on stainless steel substrates by pulsed laser deposition at 40 °C with 2–5 min deposition in 0.9 mTorr of Ar back pressure, using KrF excimer laser with an energy density of ~3–4 mJ cm^{-2} at 10 Hz impinging on the targets of Sn–Ni and Sn–Ni–SnF_2 that possess Sn:Ni ratio in 65:35 mol% and 1 mol% F, respectively. Metallic Ni is a critical component that buffers volume change during cycling [19,20]. Targets were prepared by ball-milling of Sn and Ni (and SnF_2) powders and pressing. The crystal structure of as-deposited film was determined by X-ray diffraction analysis, which was measured in the 2θ range of 10–80° with the scan rate of 2°/min using X-ray diffractometer (Rigaku D/MAX-2200). Relative Sn:Ni atomic ratio of as-deposited film was 7:3, determined using scanning electron microscopy (SEM, Jeol JSM-7000 F)-energy dispersive spectroscopy (EDS) and X-ray photoelectron spectroscopy (XPS)-depth profile (Thermo, MultiLab 2000), with Al K_α X-ray source and Ar-ion sputtering at 2 kV. High resolution spectra were obtained at a power of 150 W under a base pressure of 8×10^{-10} mbar with the pass energy of 20–30 eV. The binding energy was corrected based on the C 1*s* level at 284.7 eV.

Proto-type three-electrodes lithium cell was assembled with F-free or F-doped Sn–Ni film electrode as working electrode and lithium reference and counter electrodes in the electrolyte of 1 M $LiPF_6$/EC:EMC (3:7 volume ratio, Panax E-Tec, H_2O content 10 ppm) without and with 3 wt% trimethyl phosphite ($P(OCH_3)_3$, Aldrich) additive, respectively. As the lithium cell is a beaker-type cell, no separator was used. Their charge (lithiation) and discharge (delithiation) cycling ability was evaluated by galvanostatic cycling at 90 μA cm^{-2} (~2.4 C) in the voltage region of 0.05–1.5 V *vs.* Li/Li^+ using a multichannel cycler (Wonatech). Lithium cell assembly–disassembly and electrochemical measurement were conducted in Ar-filled glove box at room temperature.

Surface characterization for cycled electrodes was performed using *ex situ* attenuated total reflection (ATR) FTIR spectroscopy using an IR spectrometer (Nicolet 6700) equipped with a MCT detector. The cycled electrodes were separated from the cells and washed with dimethyl carbonate (DMC, Panax E-Tec) for 60 s for the removal of residual electrolyte followed by drying in the glove box at room temperature. Note that when the electrode was rinsed in DMC, soluble surface species could be washed off. The cycled electrodes were mounted on the closed ATR unit in the glove box to avoid atmospheric contamination. The SEI composition analysis was conducted using *ex situ* XPS by transferring the cycled electrodes from glove box to XPS chamber using a vacuum-sealed container without the exposure to the air.

3. Results and discussion

To identify the electronic structure of surface Sn and to probe doped F atom of pristine film electrodes, XPS analysis was conducted. Fig. 1a shows curve fitting results on the Sn $3d_{5/2}$ peak for the top surface of F-free and F-doped electrodes. The presence of surface Sn^{2+} and Sn^{4+} in addition to Sn^0 is due to tin oxides by an affinity of Sn to oxygen in the air, in particular at the surface. This mimics the characteristics of Sn active materials handled in the air. The resultant relative ratio of surface Sn^0:Sn^{2+}:Sn^{4+} is 41:39:20% for F-free electrode and 41:41:18% after F-doping, respectively. Overall, the surface valence of Sn remains similar upon low fraction F-doping. All as-deposited films consist of mainly crystalline metallic β-Sn (*I41/amd*), and a trace of metastable Ni–Sn intermetallics [19] and SnO_2 (JCPDS 75-9498), determined with XRD analysis as shown in Fig. 1b. In contrast to high oxygen content at surface, it falls to near 10% in bulk as displayed in depth-profile (Fig. 1c). High resolution F 1*s* spectrum (Fig. 1d) shows a vague spectral feature around 684–685 eV associated with SnF_2 and O-Sn-F bond [21,22]. Doped F atom seems to exist at the surface. Depth profile (Fig. 1c) shows better the presence of doped-F atom at a low fraction of 3–1 at% from surface to bulk. If F-doping occurred into SnO_2 (*e.g.*, $SnO_{2-y}F_y$), it would contribute to increase the electronic conductivity of electrode [23]. There was no F-doping effect on Ni.

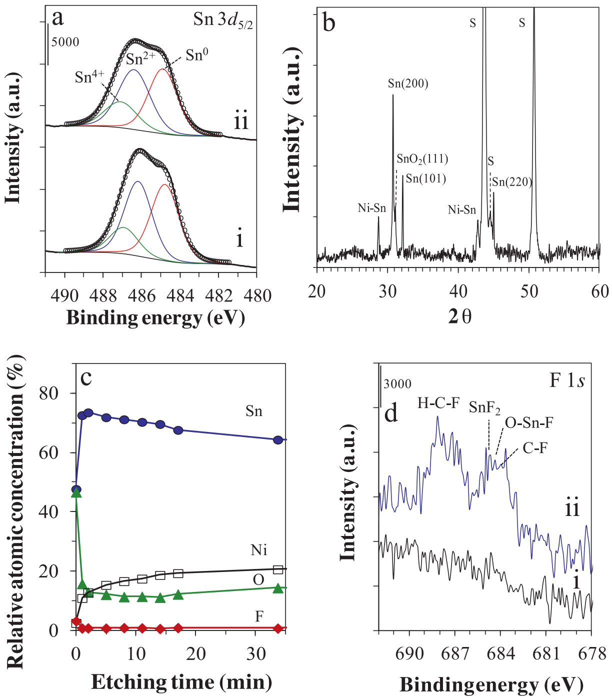

Fig. 1. XPS Sn 3*d* spectral curve fitting of pristine F-free (i) and F-doped (ii) Sn–Ni films (a), XRD pattern of pristine F-doped film (b), XPS depth profile of F-doped film (c) and F 1*s* spectral comparison of pristine F-free (i) and F-doped (ii) films (d).

Fig. 2 show voltage profiles, their d*Q*/d*V* plots (insets) and cycling ability of F-free and F-doped electrodes without and with phosphite electrolyte additive. The integrated capacities were obtained from the weight of Sn. In electrolyte only (Fig. 2a and d), F-free electrode shows low initial coulombic efficiency of 69% and a very poor cycling ability. The failure might originate from volume change-derived mechanical disintegration and interfacial degradation of the electrode. Although with phosphite additive (Fig. 2b and d) initial discharge capacity and coulombic efficiency increase to 410 mAh g^{-1} and 75%, respectively, with better cycling ability, structural resolution of lithiation and delithiation processes in d*Q*/d*V* plots tends to be diminished with cycling. The cell retains just 43% of its initial discharge capacity after 50 cycles. Significant improvement of capacity value and retention is obtained when having both F-doping combined with phosphite additive. As shown in the d*Q*/d*V* plots in the inset (Fig. 2c), structural resolution of prominent peaks by lithiation and delithiation is well maintained till the 50th cycle. Initial discharge capacity and coulombic